THEMIS IESA Moment and Velocity Distribution Corrections

Lynn B. Wilson III

August 11, 2012

Contents

1 Introduction

This software package is intended to correct the ion velocity moment returned by the TDAS routine thm_load_esa.pro that has been *contaminated* by ion beams [*e.g. Bonifazi and Moreno*, 1981a,b], gyrating ions [*e.g. Meziane et al.*, 1997], and/or gyrophase-bunched ions [*e.g. Gurgiolo et al.*, 1981]. Note that the difference between gyrating and gyrophase-bunched ions has been defined by their gyrotropy [*e.g. Fuselier et al.*, 1986] and relative distance from the terrestrial bow shock [*e.g. Meziane et al.*, 2001]. Detailed reviews of the foreshock [*e.g. Bale et al.*, 2005; *Eastwood et al.*, 2005] and upstream particle populations [*e.g. Paschmann et al.*, 1981; *Fuselier*, 1995] can be examined for further details.

All the routines in this package require both the ***UMN Modified Wind/3DP***[1] and ***THEMIS TDAS***[2] IDL libraries. The routines each have a detailed man page that explains the usage, purpose, inputs, and keywords. The man page also contains a list of routines that are called in any given program/function, as well as the routine which called said program/function. **Make sure your IDL paths are set correctly so that the routines and their dependencies can be found and compiled when called**.

1.1 Data Sets and Analysis

I will use data from fluxgate magnetometer (FGM) [*Auster et al.*, 2008] and the electrostatic analyzers (ESA) [*McFadden et al.*, 2008a,b] on the THEMIS spacecraft [*Angelopoulos*, 2008]. The data products will include the level-2 quasi-static magnetic field vector ($\mathbf{B}_o$), the level-2 ion density (n_i), the level-2 average electron temperature (T_e), the level-2 average ion temperature (T_i), the level-2 ion bulk flow velocity ($\mathbf{V}_{bulk}$), and the level-0 velocity distribution functions. The analysis will be performed in the GSE coordinate system. I will use a subscript 2 for original level-2 results and a subscript c for our "corrected" results. I limit myself to particle distributions in Burst mode herein.

The ESA instruments on THEMIS consist *...of a pair of "top hat" electrostatic analyzers with common 180° × 6° fields-of-view that sweep out 4π steradians each 3 s spin period...* [*McFadden et al.*, 2008a]. The instruments contain microchannel plate detectors that measure the energy per charge (E/q) of each incident particle. The ion (IESA) and electron (EESA) detectors were stacked together to allow for a common field-of-view (FOV). EESA(IESA) has $\Delta R/<R> \simeq 0.060(0.075)$, a measured energy resolution of $\Delta E/E$ ∼17%(∼18%), a 180°×6°(180°×6°) FOV, 8(16) anodes, anode angular resolution[3] of ∼22.5°(∼5.625°-22.5°), and spin angular resolution[4] of ∼11.25°(∼11.25°).

In Burst mode, the ESA instruments return full 4π steradian velocity distributions every spin period (∼3 seconds) with 32 energy and 88 solid angle bins per IDL structure. In-flight calibration shows that EESA(IESA) has a sensor geometric factor of ∼0.0066(0.0061) cm^2sr at a given energy. Typical analysis uses a single vector for both $\mathbf{B}_o$ and $\mathbf{V}_{bulk}$ for a single burst distribution. However, it is possible to take advantage of the high time resolution FGM data (in *fgh* mode) and effectively increase the time resolution (see Section C for details) of the distribution [*e.g. Schwartz et al.*, 2011; *Wilson III et al.*, 2012].

[1]Found at: http://tetra.space.umn.edu/wiki/doku.php/umn_wind3dp
[2]Found at: http://themis.ssl.berkeley.edu/software.shtml
[3]corresponds to the poloidal angle, θ
[4]corresponds to the azimuthal angle, ϕ

2 The Problem

2.1 Contamination Sources

Onboard particle distribution moments (or moments calculated from telemetered particle distributions) can suffer from inaccuracies due to spacecraft charging [*e.g. Génot and Schwartz*, 2004; *Geach et al.*, 2005; *Davis et al.*, 2008], multiple species [*e.g. Paschmann and Daly*, 1998], and multiple components [*e.g. Wüest, M., Evans, D. S., & von Steiger, R.*, 2007]. We must keep this in mind when examining the velocity distribution function moments.

Figure 1 shows an outbound bow shock crossing observed by THEMIS-B on 2009-07-13. The shock ramp was identified to lie between ∼08:59:45.440 UT and ∼08:59:48.290 UT and THEMIS-B was at a GSE position of ∼<+11.47, +0.98, -2.24> R_E. At first glance, one might assume that the ions are being cooled across the shock ramp when examining $T_{i,2}$ in Figure 1. In a shock crossing, the temperature should be higher on the downstream(shocked) side than upstream(unshocked). Given that the $B_{o,2}$, $V_{bulk,2}$, and $T_{e,2}$ profiles all behave as one would expect for a shock crossing, I doubt the accuracy of the $T_{i,2}$ values. I need to investigate whether the level-2 results in Figure 1 are correct.

Given that I know there are multiple ion species upstream of the terrestrial bow shock, I assume this is contributing the largest fraction of the error in the upstream $T_{i,2}$ values. The increase in density across this shock is very large, which suggests it is a very strong shock. Strong shocks that exceed a critical Mach number, M_{cr}, are predicted to require additional energy dissipation in the form of particle reflection to limit wave steepening [*e.g. Edmiston and Kennel*, 1984]. Therefore, I can assume that some fraction of the error in the moments is due to reflected ion populations like field-aligned beams [*e.g. Bonifazi and Moreno*, 1981a,b], gyrating ions [*e.g. Meziane et al.*, 1997], or gyrophase-bunched ions [*e.g. Gurgiolo et al.*, 1981]. To test whether ion beams do exist upstream of the shock ramp, I need to examine the entire ion velocity distribution functions in the bulk flow rest frame.

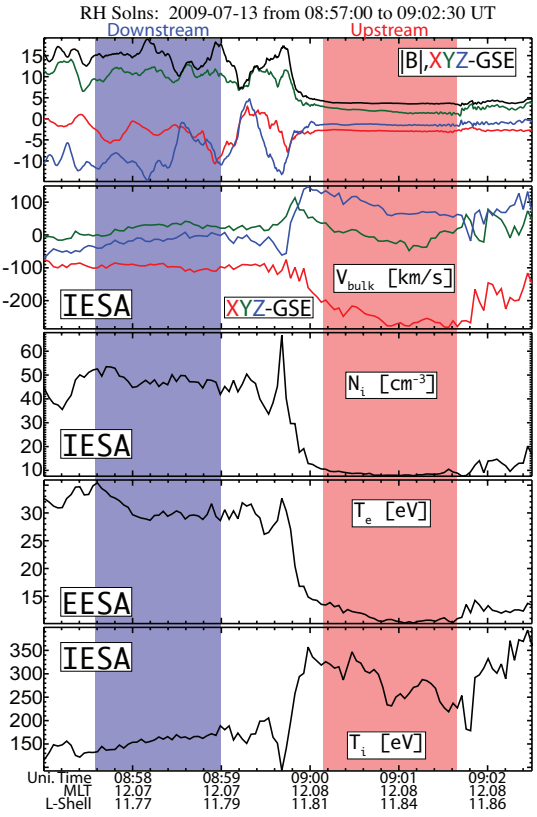

Figure 1: The figure shows an example bow shock crossing with the smoothed $\mathbf{B}_{o,2}$ and $B_{o,2}$ (nT, first panel), $\mathbf{V}_{bulk,2}$ (km/s, second panel), $n_{i,2}$ (cm^{-3}, third panel), $T_{e,2}$ (eV, fourth panel), and $T_{i,2}$ (eV, fifth panel). The region shaded in blue I defined as downstream (*i.e.* magnetosheath) and red as upstream (*i.e.* solar wind). The data was measured by THEMIS-B.

2.2 Velocity Distribution Plots

Examination of the particle velocity distribution functions can be done in various ways, but I have found the following to work best for myself:

1. Retrieve *THEMIS* IESA Burst particle distributions
2. Transform into the original level–2 bulk flow reference frame [5]
3. Rotate the (energy,θ,ϕ)-bins into a field-aligned coordinate system and triangulate the data onto the three planes defined by this new basis
4. Smooth the results to fill NaNs or data gaps and improve IDL's ability to plot the data
5. Plot the data as contours of constant phase (velocity) space density versus the velocities along the directions defined by the plane of projection you wish to examine
6. Plot cuts of the data (with one-count level[6]) to aid in analysis/interpretation as well to help with a better constraint on the Z-Axis range
7. Look for evidence of free energy[7] in the particle distributions or evidence of heating/acceleration.

Some may prefer to examine the distributions in the spacecraft frame, but as I will show shortly, this can cause misleading results or misinterpretation of the analysis. Examination of the distributions in the bulk flow frame looking at the entire distribution is something that is far too often overlooked in favor of the much easier and quicker examination of velocity moments. However, as Figure 1 shows, interpretation based upon velocity moments alone without examination of the entire distribution in velocity space or an understanding of the sources of error/contamination would result in incorrect conclusions. Below, I illustrate why the analysis of the distributions should not be limited to velocity moments when plots like those shown in Figure 2 can be easily produced.

Figure 2 shows an example ion velocity distribution in two different bulk flow rest frames[8], defined by $\mathbf{V}_{bulk}$. The left-hand column of contours show the distribution in the rest frame defined by $\mathbf{V}_{bulk,2}$ (level-2 velocity moments shown in Figure 1). One can see that the peak (red contours) is not centered on zero velocity in any of the three planes. The middle column shows the distribution in a "corrected" rest frame, where I adjusted $\mathbf{V}_{bulk,2}$ so the peak of the distribution would be at zero velocity giving us $\mathbf{V}_{bulk,c}$. One can see that there are significant intensities of ion beams anti-parallel to $\mathbf{B}_{o,2}$, with a broad range of pitch-angles between ∼500-900 km/s. The square-like region of red contours near ∼400 km/s in each contour in the middle panel is due to UV contamination[9]. I observe significant gyrating and field-aligned ion beams throughout the entire upstream region.

I should note that the nonthermal features shown in Figure 2 can be significantly different if I use multiple values of $\mathbf{B}_{o,2}$ per distribution to determine higher time resolution pitch-angle distributions (see Section C). The center of the *core*, however, appears to be relatively stable on spin period (∼3 seconds) time scales allowing us to use the corrected $\mathbf{V}_{bulk}$ found in the next section for a transformation velocity. The changes due to the higher time resolution are more dramatic for IESA than EESA due to longer gyroperiod of ions. I should also state that the IESA Burst distributions observed during this shock crossing were not in solar wind mode.

[5] use the velocity shown in Figure 1 for initial analysis
[6] this is for statistics and informs the user whether the data is significant or instrumental noise
[7] the energy available that can do work on a system
[8] In the coordinate systems defined in the far right column, $\mathbf{V}_{bulk} = \mathbf{V}_{sw}$.
[9] Found in the following quadrants from top-to-bottom: third, second, and fourth

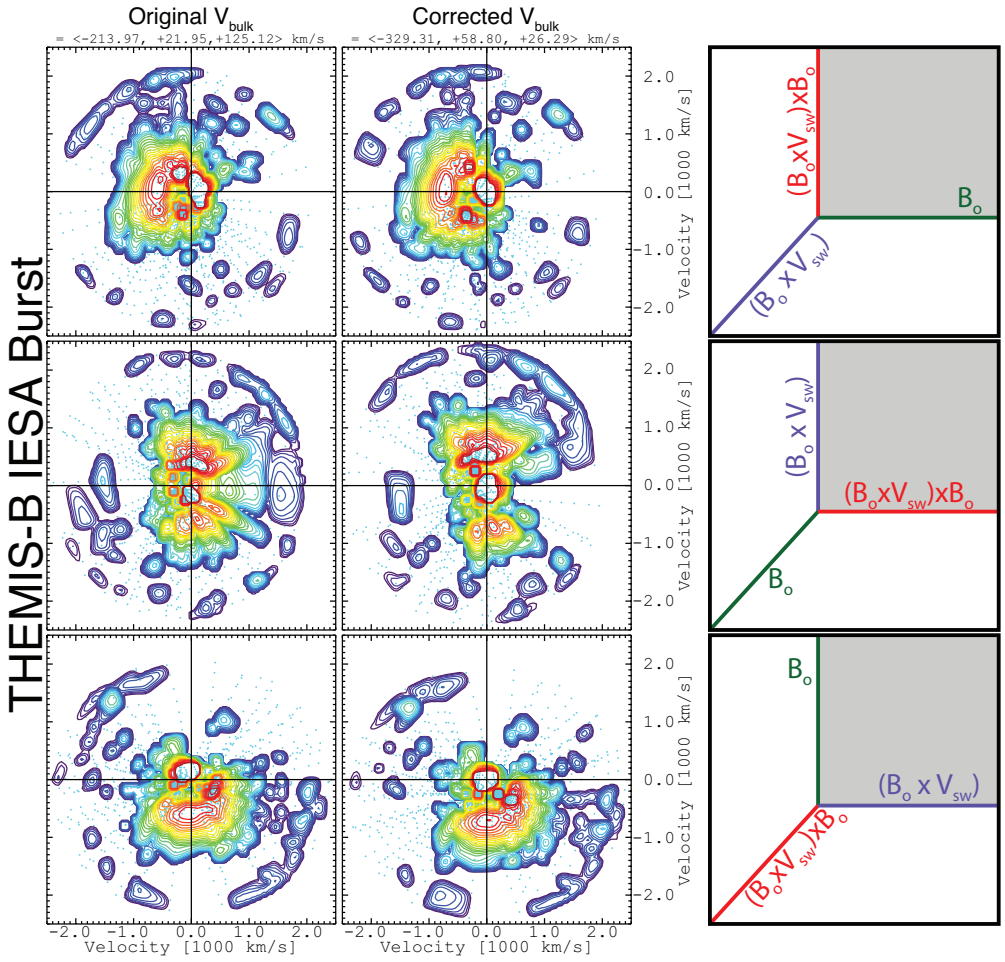

Figure 2: An example IESA Burst particle velocity distribution observed upstream of the corresponding shock ramp in Figure 1 at ∼09:00:12 UT. The two columns of contour plots correspond to two different rest frames defined by $\mathbf{V}_{bulk}$ at the top of each column. Each contour plot shows contours of constant phase space density (uniformly scaled from $1{\times}10^{-14}$ to $1{\times}10^{-8}$ $s^3cm^{-3}km^{-3}$, where red is high) versus velocity projected onto three different planes defined by the shaded region in the coordinate axes shown in right-hand column. The velocity axes range from ±2500 km/s and the crosshairs show the location of the origin.

2.3 Velocity Distribution Masks

After finding the correct bulk flow rest frames, $\mathbf{V}_{bulk,c}$, I were able to isolate the *core* of the ion distribution from the beam components. I created a mask that would eliminate all the ions outside the *core* component. I also removed ions within a small cone around the sun direction to reduce the effects of UV contamination. The mask was only applied to those distributions with well defined beam components[10]. Then I took this new distribution and re-performed the moment analysis.

Figure 3 shows the same time range as in Figure 1, but now compares the original level-2 results

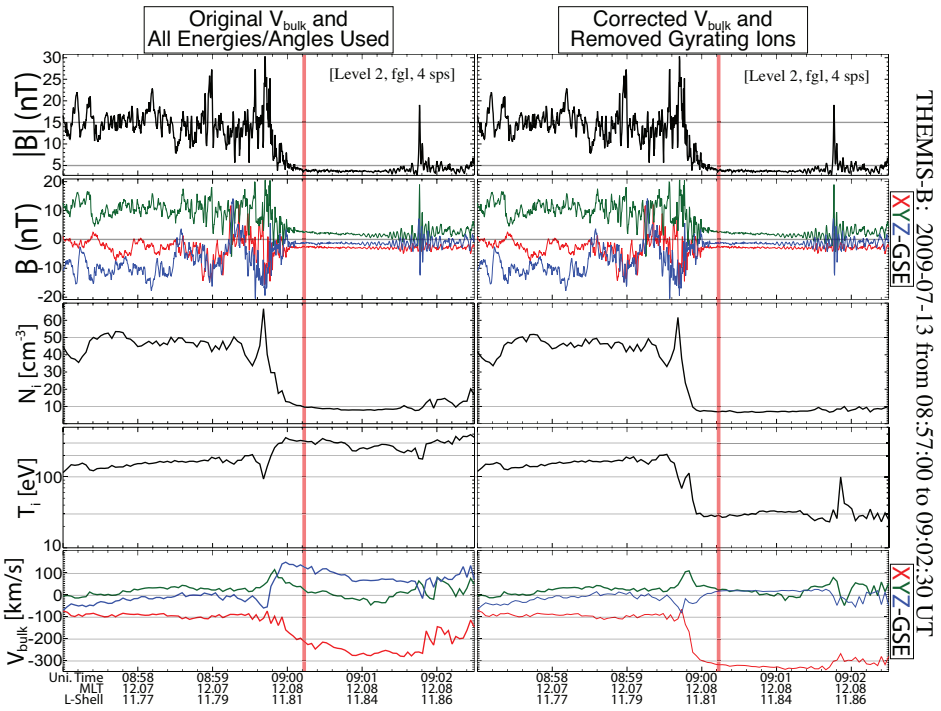

Figure 3: This figure compares the original level-2 moments (left-hand column) to our corrected estimates (right-hand column). The panels are as follows: B_o (nT, first panel), $\mathbf{B}_o$ (nT, second panel), n_i (cm^{-3}, third panel), T_i (eV, fourth panel), and $\mathbf{V}_{bulk}$ (km/s, fifth panel). Note that the magnetic field estimates in each column are identical. The horizontal gray lines in each panel are to help the reader compare the two results. The red shaded region corresponds to the time range of the ion velocity distribution in Figure 2.

(left-hand column) to our "corrected" results[11] (right-hand column). I also show the magnetic field at four samples per second without smoothing to show the large variability of this event. Notice that T_i now increases across the shock ramp and that $\Delta V_{bulk,c} > \Delta V_{bulk,2}$. There is a slight decrease in n_i where beam components were present, as expected. One can see that the large amplitude fluctuation[12] in B_o near ~09:01:48 UT appears to heat and deflect the *core* ions, and increase the relative abundance of beam ions, consistent with recent observations.

[10]Note that this required that I produce plots like those shown in Figure 2 for every distribution and examine them by eye.

[11]These produced after $\mathbf{V}_{bulk}$ correction and after the moment analysis done on the distributions with an applied mask.

[12]The feature looks similar to a short large amplitude magnetic structure (SLAMS), but it may also be another bow shock crossing. Shortly after (~1 minute) this feature, the bow shock expanded and the spacecraft was re-immersed in the magnetosheath.

These plots show that the abundance of beam ions can significantly alter the results produced during moment analysis, whether onboard or ground calculations. The purpose of this section is to illustrate why it is important to always analyze particle distributions using tools like that shown in Figure 2. The use of particle moments without examination of the velocity distribution function in phase (velocity) space can be, as shown herein, very misleading. While the data product may be at level-2 status, I have clearly shown that such products can be contaminated causing errors greater than a factor of three above the *true* values (*e.g.* see T_i in Figure 3).

Further examination of the distributions in Figure 2 show that the beam component can be non-gyrotropic, which introduces off-diagonal terms in the second moment (*i.e.* the pressure tensor) [*e.g. Gedalin and Zilbersher*, 1995]. A primary concern is the use of moment analysis to estimate instability thresholds. If one does not account for these non-gyrotropic features the results will be misleading and this could cause inappropriate conclusions in published works. The problems associated with moment analysis conducted on measured velocity space distributions in space plasmas have been well known since their inception. However, I wonder how many authors have thoroughly examined the entire distributions in velocity space?

3 IDL Routines

3.1 Process Overview

3.1.1 Correcting Bulk Flow Velocity

This software is intended for the *THEMIS* ion particle distributions. The software used assumes the maximum peak of the distribution corresponds to the center of the *core* of the ion distribution. If the source of error is due to ion beams, whether field-aligned or gyrating, then their maximum phase (velocity) space density should be less than the *core* part. Therefore, the routine fix_vbulk_ions.pro finds the peak in phase (velocity) space density and then determines the corresponding velocity. The crib sheet, themis_esa_correct_bulk_flow_crib.txt, outlines the steps to correct the velocity moment. The steps are as follows:

1. Retrieve *THEMIS* IESA Burst particle distributions (*e.g.* call themis_load_fgm_esa_inst.pro)
2. Modify data structures so they are compatible with the ***UMN Modified Wind/3DP*** software (*e.g.* call modify_themis_esa_struc.pro)
3. Rotate (θ,ϕ)-angles from DSL to GSE coordinates (call rotate_esa_thetaphi_to_gse.pro)
4. Make sure each structure has finite values for the tags MAGF, VSW, and SC_POT by calling add_magf2.pro, add_vsw2.pro, and add_scpot.pro using the keyword **LEAVE_ALONE**
5. Transform into original level–2 bulk flow reference frame (call transform_vframe_3d.pro)
6. Find the velocity associated with peak in phase (velocity) space density in this frame of reference (call fix_vbulk_ions.pro)
7. Remove *data spikes* in new transformation velocity due to "bad" peaks in the distributions
8. Smooth the resulting velocities and send the result to TPLOT
9. Plot the data and remove any remnant *data spikes* manually (call kill_data_tr.pro), get the data (call get_data.pro), linearly interpolate to fill NaNs (call interp.pro), and send back to TPLOT[13] (call store_data.pro)
10. Save the TPLOT session for reproducibility (call tplot_save.pro)

3.1.2 Removing Beam Components

This software is intended for the *THEMIS* ion particle distributions. The software creates a mask (remove_uv_and_beam_ions.pro) that corresponds to the data bins not within the *core*. Once the mask is applied to the *contaminated* energy/angle data bins, the distributions can be re-analyzed using the moment analysis software (*e.g.* moments_3du.pro). The crib sheet, themis_esa_correct_moments_crib.txt, outlines the steps to correct the velocity moment. The steps are as follows:

1. Retrieve *THEMIS* IESA Burst particle distributions (*e.g.* call themis_load_fgm_esa_inst.pro)
2. Modify data structures so they are compatible with the ***UMN Modified Wind/3DP*** software (call modify_themis_esa_struc.pro)

[13] This step may need to be repeated multiple times...

3. Rotate (θ,ϕ)-angles from DSL to GSE coordinates (call rotate_esa_thetaphi_to_gse.pro)

4. Make sure each structure has finite values for the tags MAGF, VSW[14], and SC_POT by calling add_magf2.pro, add_vsw2.pro, and add_scpot.pro using the keyword **LEAVE_ALONE**. The mask routine will convert the input structures into the bulk flow rest frame prior to determining the elements to mask.

5. **Create a Mask** (remove_uv_and_beam_ions.pro)

   (a) Define all the time ranges that are contaminated by ion beams, gyrating or gyrophase-bunched ions by plotting all the distributions in your time of interest (*e.g.* call contour_3d_1plane.pro or contour_esa_htr_1plane.pro)

   (b) From the contour plots, determine the lowest acceptable speed ($V_{thresh} \Rightarrow$ V_THRESH keyword) that is not contaminated with beam component ions

   (c) From the contour plots, determine the largest speed affected by UV light ($V_{uv} \Rightarrow$ V_UV keyword)

   (d) Call remove_uv_and_beam_ions.pro, where the result will be an [$N_E \times N_A \times N_D$]-element array, where N_E = # of energy bins per data structure (32/spin in Burst mode), N_A = # of angle bins per data structure (88/spin in Burst mode), and N_D = # of IDL data structures (one for each IESA Burst particle distribution)

6. Apply mask to contaminated ion distributions[15] in the following way:

```
THEMIS> dummy  = data_arr;; Create dummy copy
THEMIS> dumbd  = dummy.DATA
THEMIS> mask   = remove_uv_and_beam_ions(dummy,V_THRESH=v_thresh,V_UV=v_uv)
;; apply mask
THEMIS> dumbd *= mask
THEMIS> dummy.DATA = dumbd
```

7. Find elements of DATA_ARR that are contaminated and replace them with the corresponding elements of DUMMY by using the previously determined time ranges

8. Recalculate the particle moments (*e.g.* call moments_3du.pro) on the original structure in GSE coordinates in the spacecraft frame

9. Send results to TPLOT and compare the new $\mathbf{V}_{bulk}$ produced by this new moment analysis (*e.g.* lower right-hand corner of Figure 3) with the $\mathbf{V}_{bulk}$ produced from the steps in Section 3.1.1 and the original level-2 result (*e.g.* lower left-hand corner of Figure 3)

10. Save the TPLOT session for reproducibility (call tplot_save.pro)

3.2 Main Routines

The two routines that correct the ion moments are
fix_vbulk_ions.pro and
remove_uv_and_beam_ions.pro. Both routines require the ***UMN Modified Wind/3DP*** software package.

IDL Routine Inputs

The required inputs for fix_vbulk_ions.pro are:

[14] Make sure the TPLOT handle you use is associated with the corrected bulk flow velocity determined from the steps in Section 3.1.1.

[15] let DATA_ARR be the N_D-element array of data structures in the spacecraft frame in GSE coordinates

1. **DAT** = A scalar data structure from THEMIS IESA [see get_pei?.pro, thm_part_dist_array.pro, *etc.*] in Burst mode

IDL Routine Keywords

The keywords are:

1. **NSMOOTH** = Scalar defining the # of data points over which to smooth the particle distribution prior to finding the *core* peak

IDL Routine Inputs

The required inputs for remove_uv_and_beam_ions.pro are:

1. **DAT** = An N_D-element array of data structures from THEMIS IESA [see get_pei?.pro, thm_part_dist_array.pro, *etc.*] in Burst mode

IDL Routine Keywords

The keywords are:

1. **V_THRESH** = Scalar defining the largest velocity [km/s] that is not contaminated by an ion beam component [Default = 500]
2. **V_UV** = Scalar defining the largest velocity [km/s] that is affected by UV light [Default = 500]
3. **THE_THR** = Scalar defining the largest poloidal angle [degrees] away from the sun direction to be removed due to UV light contamination [Default = 15°]
4. **PHI_THR** = Scalar defining the largest azimuthal angle [degrees] away from the sun direction to be removed due to UV light contamination [Default = 15°]

3.3 Crib Sheets

An example of how to "correct" $\mathbf{V}_{bulk}$ is shown in themis_esa_correct_bulk_flow_crib.txt found in the *~/wind_3dp_pros/wind_3dp_cribs/* directory. Follow the steps and change the dates/times and directory paths as necessary. One can use this estimate to help create the mask in the next step to further improve the estimate of $\mathbf{V}_{bulk}$.

To remove the beam components and UV light contamination from the distributions, follow the steps shown in themis_esa_correct_moments_crib.txt. Again, change the dates/times and directory paths as necessary. The new $\mathbf{V}_{bulk}$ produced from the moment analysis (*i.e.* steps in Section 3.1.2) after applying the mask should be more accurate than the previous "corrected" version, which can be seen when comparing all three versions of the variable in TPLOT.

A Particle Data Structures in IDL

Full 3-dimensional particle distributions from the ESA instruments come as data structures in the TDAS software [*McFadden et al.*, 2008a]. The list of structure tags includes (but is not limited to), in no particular order:

1. **PROJECT_NAME** ≡ scalar [string] *e.g.* 'THEMIS-B'
2. **SPACECRAFT** ≡ scalar [string] *e.g.* 'b'
3. **DATA_NAME** ≡ scalar [string] *e.g.* 'IESA 3D burst'[16]
4. **UNITS_NAME** ≡ scalar [string] *e.g.* 'counts'[17]
5. **UNITS_PROCEDURE** ≡ scalar [string] (*e.g.* 'thm_convert_esa_units') that tells conv_units.pro which IDL routine to use to convert the data units
6. **TIME** ≡ scalar [double] defining the Unix[18] time associated with start of data sample (might be a slight delay from the sun pulse timestamp)
7. **END_TIME** ≡ scalar [double] defining the Unix time associated with end of data sample
8. **DELTA_T** ≡ scalar [double] defining total duration of IDL structure [= END_TIME - TIME]
9. **INTEG_T** ≡ scalar [double] defining the average time needed for the 1024 counter readouts per spin (s) [= (END_TIME - TIME)/1024]
10. **NENERGY** ≡ scalar [integer] defining the number of energy bins
11. **NBINS** ≡ scalar [integer] defining the number of solid angle bins
12. **DT_ARR** ≡ [NENERGY,NBINS]-element array [float] of anode accumulation times [unitless] per bin ⇒ accumulation time [s] of any given bin = (INTEG_T * DT_ARR)
13. **DATA** ≡ [NENERGY,NBINS]-element array [float] defining the data point values for each energy/angle bin [units depend on the value of UNITS_NAME]
14. **ENERGY** ≡ [NENERGY,NBINS]-element array [float] of average energy bin values [eV]
15. **DENERGY** ≡ [NENERGY,NBINS]-element array [float] defining the energy range [eV] of each value of ENERGY
16. **PHI** ≡ [NENERGY,NBINS]-element array [float] defining the average azimuthal angle[19] [deg] for each bin
17. **DPHI** ≡ [NENERGY,NBINS]-element array [float] defining the angular range(uncertainty) [deg] for each value of PHI
18. **THETA** ≡ [NENERGY,NBINS]-element array [float] defining the average poloidal angle[20] [deg] for each bin

[16] see dat_themis_esa_str_names.pro for more possibilities
[17] see thm_convert_esa_units_lbwiii.pro for descriptions and more possibilities
[18] seconds since January 1, 1970
[19] $+95^\circ \lesssim \theta \lesssim +450^\circ$ in DSL coordinates, where $+180^\circ$ is roughly in the sun direction
[20] $-90^\circ \leq \theta \leq +90^\circ$, where 0° is roughly in the spin plane

19. **DTHETA** ≡ [NENERGY,NBINS]-element array [float] defining the angular range(uncertainty)[21] [deg] for each value of DTHETA

20. **EFF** ≡ [NENERGY,NBINS]-element array [double] defining the efficiency correction [unitless] to the geometry factor accounting for dead time corrections

21. **GEOM_FACTOR** ≡ scalar [float] defining the total geometry factor of the detector [cm^2sr]

22. **GF** ≡ [NENERGY,NBINS]-element array [float] defining the relative geometric factor per bin ⇒ the geometry factor of each bin is = (GEOM_FACTOR * GF * EFF)

23. **DEAD** ≡ scalar [float] defining the detector dead time [∼170 ± 10 ns] of the Amptek A121 preamplifier[22]

24. **CHARGE** ≡ scalar [float] defining the sign of the particle charge being measured

25. **MASS** ≡ scalar [float] defining the mass [$(eV/c)^2$ with c in km/s] of the particles being measured

26. **MAGF** ≡ [3]-element array [float] defining the average magnetic field vector [nT] for the duration of the distribution (coordinate system depends on user preference but should match the basis defining PHI and THETA to be meaningful and useful)

27. **VELOCITY** ≡ [3]-element array [double] defining the average bulk flow velocity [km/s] for the duration of the distribution (coordinate system issue similar to MAGF)

28. **SC_POT** ≡ scalar [float] defining the estimate of the spacecraft potential (eV)

B Unit Conversions

To convert between different units[23], a few quantities must be calculated first. Let us assume we start with the units of counts. Let us assume we have a particle distribution IDL data structure called *dat* (see Section A for structure tag definitions), then we can define the following quanties:

1. E ≡ particle kinetic energy (eV) [associated with dat.ENERGY]

2. N_E ≡ number of energy bins [associated with dat.NENERGY]

3. N_A ≡ number of solid angle bins [associated with dat.NBINS]

4. δt ≡ sample/accumulation time (s) [associated with dat[0].INTEG_T[0]*dat.DT_ARR]

5. gf ≡ differential geometry factor for each data point [associated with dat.GF * dat.GEOM_FACTOR * dat.EFF]

6. M_s ≡ particle mass of species s ($(eV/c)^2$ with c in km/s) [associated with dat.MASS]

7. τ ≡ dead time [associated with dat.DEAD]

8. $f(E,\Omega)$ ≡ the data [associated with dat.DATA in counts], where Ω is the solid angle

9. $g(E,\Omega)$ ≡ the data in new user specified units

[21] this is limited primarily by the anodes being used in a particular mode
[22] see, for example, *Paschmann and Daly* [1998] for explanation of dead times
[23] see, for example, thm_convert_esa_units_lbwiii.pro

10. $\delta g \equiv$ estimated uncertainty in *g(E,Ω)*

To correct for the dead time, we define:

$$\delta t_c \equiv \frac{\tau f(E,\Omega)}{\delta t} \tag{1}$$

The scale factors used to convert from counts to any of the following are:

$$Counts : scale = 1.0 \tag{2a}$$
$$rate : scale = (\delta t)^{-1} \tag{2b}$$
$$crate : scale = (\delta t)^{-1} \tag{2c}$$
$$eflux : scale = (\delta t * gf)^{-1} \tag{2d}$$
$$flux : scale = (\delta t * gf * E)^{-1} \tag{2e}$$
$$df : scale = (\delta t * gf * E)^{-1} * \left(\frac{mass^2}{2.0 \times 10^5}\right) \tag{2f}$$

where the final result in new units is given by:

$$g(E,\Omega) = scale * \left(\frac{f(E,\Omega)}{\delta t_c}\right) \ . \tag{3}$$

The uncertainty in *g(E,Ω)* is given by:

$$\delta g = scale * \left(\frac{f(E,\Omega)}{\delta t_c}\right)^{1/2} \ . \tag{4}$$

C Increased Time Resolution

Each ESA Burst data structure requires a spin period (∼3 seconds) to sample their entire 4π steradians and energy range. So the standard practice is to use one magnetic field and bulk flow velocity vector per particle distribution during analysis. I know from observations that the magnetic field fluctuates on time scales (spacecraft frame) much less than a spin period. The question then is, do the particles respond on the same time scales as the magnetic field?

To investigate this, let us use the notations from Section B in addition to the following:

1. $\phi_{i,j} \equiv$ average azimuthal angle[24] (deg) of the (i^{th},j^{th})-data bin [associated with dat.PHI]
2. $\theta_{i,j} \equiv$ average poloidal angle (deg) (i^{th},j^{th})-data bin [associated with dat.THETA]
3. $t_s \equiv$ start time of distribution [associated with dat.TIME]
4. $t_e \equiv$ end time of distribution [associated with dat.END_TIME]
5. $\Delta t = t_e$ - t_s (seconds)
6. $T_{sc} \equiv$ spin period of spacecraft (seconds)
7. $\tilde{t}_{int} \equiv$ average time needed for the 1024 counter readouts per spin (seconds) [associated with dat.INTEG_T] $\mathcal{T}_{i,j} \equiv$ accumulation time (seconds) of the (i^{th},j^{th})-data bin [defined by dat.INTEG_T*dat.DT_ARR]

[24] both θ and ϕ **MUST** be in the DSL basis

We define the azimuthal start angle, $\phi_{0,0}$, of the distribution and shift the rest of the azimuthal angles:

$$\tilde{\phi}_{i,j} = \phi_{i,j} - \phi_{0,0} \tag{5}$$

Since $\phi_{0,0} \neq 0°$ by default, we adjust the new shifted angles by:

$$\tilde{\phi}' = \tilde{\phi} + 360° \tag{6a}$$

$$\tilde{\phi}'' = \tilde{\phi}' - MIN\left(\tilde{\phi}'\right) \tag{6b}$$

so that the smallest angle of $\tilde{\phi}$" $= 0°$. Now we define the spin rate [deg/s] by:

$$\omega_{sc} = \frac{360°}{T_{sc}} \tag{7}$$

and we divide our shifted angles by ω_{sc} to get the time difference between the (i^{th},j^{th})-data bin and the first data point, $\Delta t_{i,j}$ ($= \tilde{\phi}"_{i,j}/\omega_{sc}$). Note that each $\Delta t_{i,j}$ is actually half an accumulation time from the *true* start time of the (i^{th},j^{th})-data bin, so we define:

$$\Delta t'_{i,j} = \Delta t_{i,j} + \mathcal{T}_{i,j} \ . \tag{8}$$

Finally, we arrive at the answer we seek, the Unix timestamp associated with (i^{th},j^{th})-data bin given by:

$$t_{i,j} = t_s + \Delta t'_{i,j} \ . \tag{9}$$

Now that we have timestamps for each energy/angle bin in the particle distribution, we can use the high time resolution (≤128 samples/s) magnetometer data to determine the pitch-angle for the (i^{th},j^{th})-data bin. The end result is a reduction in the time-aliasing that occurs when sampling a velocity distribution over long (∼3 seconds) periods of time compared to gyration periods, fluctuation periods, convection time scales, *etc.* Note that this is a crude method and that the data in any given azimuth is sampled from $\phi_{i,j}$ - $\Delta\phi_{i,j}$ to $\phi_{i,j}$ + $\Delta\phi_{i,j}$ during a time $\mathcal{T}_{i,j}$. A more accurate algorithm would involve finding the magnetic field data within $t_s \pm \Delta t'_{i,j}/2$ and taking the average. Of course, all of this assumes that the spin period is well defined and constant and that t_s corresponds to the *true* start time of the distribution associated with the sun pulse signal. Even so, the technique can reveal non-gyrotropic features that are *smeared* out in velocity space when using the standard technique, which are important for instability analysis and comparisons to theory/simulation.

To utilize this technique, see the following routines:
timestamp_esa_angle_bins.pro,
rotate_esa_htr_structure.pro, and
contour_esa_htr_1plane.pro
in the ∼*/wind_3dp_pros/THEMIS_PRO/* directory. An example of the usage of these routines can be found in the crib sheet themis_esa_contour_plots_crib.txt in the ∼*/wind_3dp_pros/wind_3dp_cribs/* directory.

References

Angelopoulos, V. (2008), The THEMIS Mission, *Space Sci. Rev.*, *141*, 5–34, doi:10.1007/s11214-008-9336-1.

Auster, H. U., et al. (2008), The THEMIS Fluxgate Magnetometer, *Space Sci. Rev.*, *141*, 235–264, doi:10.1007/s11214-008-9365-9.

Bale, S. D., et al. (2005), Quasi-perpendicular Shock Structure and Processes, *Space Sci. Rev.*, *118*, 161–203, doi:10.1007/s11214-005-3827-0.

Bonifazi, C., and G. Moreno (1981a), Reflected and diffuse ions backstreaming from the earth's bow shock. I Basic properties, *J. Geophys. Res.*, *86*, 4397–4413, doi:10.1029/JA086iA06p04397.

Bonifazi, C., and G. Moreno (1981b), Reflected and diffuse ions backstreaming from the earth's bow shock 2. Origin, *J. Geophys. Res.*, *86*, 4405–4414, doi:10.1029/JA086iA06p04405.

Davis, V. A., M. J. Mandell, and M. F. Thomsen (2008), Representation of the measured geosynchronous plasma environment in spacecraft charging calculations, *J. Geophys. Res.*, *113*, 10,204, doi:10.1029/2008JA013116.

Eastwood, J. P., E. A. Lucek, C. Mazelle, K. Meziane, Y. Narita, J. Pickett, and R. A. Treumann (2005), The Foreshock, *Space Sci. Rev.*, *118*, 41–94, doi:10.1007/s11214-005-3824-3.

Edmiston, J. P., and C. F. Kennel (1984), A parametric survey of the first critical Mach number for a fast MHD shock., *J. Plasma Phys.*, *32*, 429–441.

Fuselier, S. A. (1995), Ion distributions in the Earth's foreshock upstream from the bow shock, *Adv. Space Res.*, *15*, 43–52, doi:10.1016/0273-1177(94)00083-D.

Fuselier, S. A., M. F. Thomsen, J. T. Gosling, S. J. Bame, and C. T. Russell (1986), Gyrating and intermediate ion distributions upstream from the earth's bow shock, *J. Geophys. Res.*, *91*, 91–99, doi:10.1029/JA091iA01p00091.

Geach, J., S. J. Schwartz, V. Génot, O. Moullard, A. Lahiff, and A. N. Fazakerley (2005), A corrector for spacecraft calculated electron moments, *Ann. Geophys.*, *23*, 931–943, doi:10.5194/angeo-23-931-2005.

Gedalin, M., and D. Zilbersher (1995), Non-diagonal ion pressure in nearly-perpendicular collisionless shocks, *Geophys. Res. Lett.*, *22*, 3279–3282, doi:10.1029/95GL03284.

Génot, V., and S. Schwartz (2004), Spacecraft potential effects on electron moments derived from a perfect plasma detector, *Ann. Geophys.*, *22*, 2073–2080, doi:10.5194/angeo-22-2073-2004.

Gurgiolo, C., G. K. Parks, B. H. Mauk, K. A. Anderson, R. P. Lin, H. Reme, and C. S. Lin (1981), Non-E x B ordered ion beams upstream of the earth's bow shock, *J. Geophys. Res.*, *86*, 4415–4424, doi:10.1029/JA086iA06p04415.

McFadden, J. P., C. W. Carlson, D. Larson, M. Ludlam, R. Abiad, B. Elliott, P. Turin, M. Marckwordt, and V. Angelopoulos (2008a), The THEMIS ESA Plasma Instrument and In-flight Calibration, *Space Sci. Rev.*, *141*, 277–302, doi:10.1007/s11214-008-9440-2.

McFadden, J. P., C. W. Carlson, D. Larson, J. Bonnell, F. Mozer, V. Angelopoulos, K.-H. Glassmeier, and U. Auster (2008b), THEMIS ESA First Science Results and Performance Issues, *Space Sci. Rev.*, *141*, 477–508, doi:10.1007/s11214-008-9433-1.

Meziane, K., et al. (1997), Wind observation of gyrating-like ion distributions and low fre-

quency waves upstream from the earth's bow shock, *Adv. Space Res.*, *20*, 703–706, doi:10.1016/S0273-1177(97)00459-6.

Meziane, K., C. Mazelle, R. P. Lin, D. LeQuéau, D. E. Larson, G. K. Parks, and R. P. Lepping (2001), Three-dimensional observations of gyrating ion distributions far upstream from the Earth's bow shock and their association with low-frequency waves, *J. Geophys. Res.*, *106*, 5731–5742, doi:10.1029/2000JA900079.

Paschmann, G., and P. W. Daly (1998), Analysis Methods for Multi-Spacecraft Data. ISSI Scientific Reports Series SR-001, ESA/ISSI, Vol. 1. ISBN 1608-280X, 1998, *ISSI Sci. Rep. Ser.*, *1*.

Paschmann, G., N. Sckopke, I. Papamastorakis, J. R. Asbridge, S. J. Bame, and J. T. Gosling (1981), Characteristics of reflected and diffuse ions upstream from the earth's bow shock, *J. Geophys. Res.*, *86*, 4355–4364, doi:10.1029/JA086iA06p04355.

Schwartz, S. J., E. Henley, J. Mitchell, and V. Krasnoselskikh (2011), Electron Temperature Gradient Scale at Collisionless Shocks, *Phys. Rev. Lett.*, *107*, 215,002, doi:10.1103/PhysRevLett.107.215002.

Wilson III, L. B., et al. (2012), Observations of Electromagnetic Whistler Precursors at Supercritical Interplanetary Shocks, *Geophys. Res. Lett.*, *39*, L08,109–+, doi:10.1029/2012GL051581.

Wüest, M., Evans, D. S., & von Steiger, R. (Ed.) (2007), *Calibration of Particle Instruments in Space Physics*, ESA Publications Division, Keplerlaan 1, 2200 AG Noordwijk, The Netherlands.